CENTER FOR ASTROPHYSICS
HARVARD & SMITHSONIAN

Submillimeter Array Newsletter

Number 29, January 2020

CONTENTS

FROM THE DIRECTOR

Dear SMA Newsletter readers,

I am happy to announce that the intermediate upgrade to further increase the bandwidth of the SMA is progressing well, with all receivers in all antennas now capable of producing an IF band covering 4 to 16 GHz. This translates to an instantaneous on-sky spectral coverage of up to 48 GHz for different receiver tunings, or 24 GHz for dual polarization with increased sensitivity. The maximum contiguous coverage with the current system is 44 GHz, which includes 4 GHz spectral overlap of the two polarizations. This setup is demonstrated in the test spectrum below, from 1 of 21 baselines, obtained towards Orion KL during science commissioning of quadrants 5 and 6 of the SWARM correlator. Science commissioning is proceeding well, and we expect to offer the increased bandwidth in the upcoming call for observing proposals for semester 2020A, which begins May 16th. Please join me in thanking the many staff members in Hilo, Cambridge, and Taipei who made this happen.

Ray Blundell

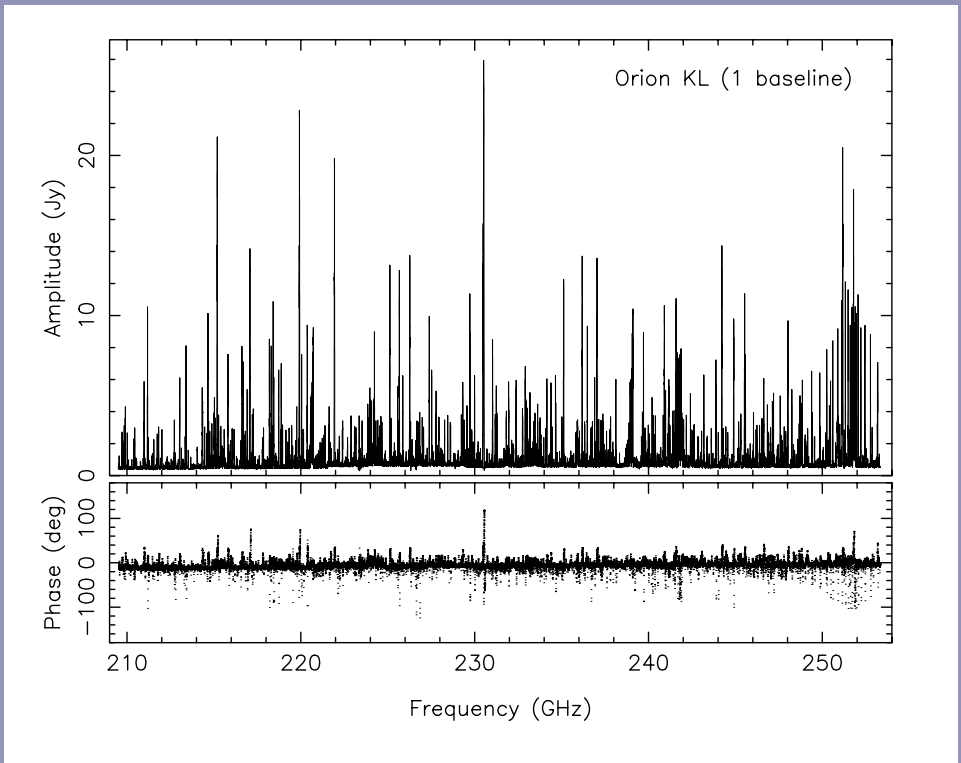

DISCOVERY OF A DOZEN TORSIONALLY-EXCITED METHANOL MASER LINES DURING A TRANSIENT FLARE IN THE MASSIVE PROTOSTAR G358.93-0.03 MM1

Todd R. Hunter (NRAO), Crystal L. Brogan (NRAO), Allison P. M. Towner (UVA), Mark A. Gurwell (CfA), Naomi Hirano (ASIAA), Gordon C. MacLeod (HartRAO), T.K. Sridharan (CfA), and the M2O Collaboration

It has been long recognized (Kenyon et al. 1990) that time variable accretion may provide a key ingredient to solving the "luminosity problem", in which surveys of low mass protostars show lower mean luminosities than expected from theory (Evans et al. 2009, Offner & McKee 2011, Hartmann, Herczeg & Calvet 2016). In recent years, SMA observations have contributed to the growing body of evidence that episodic accretion is indeed a common mechanism in the formation of low mass stars, yielding intervals of elevated luminosity (Frimann et al. 2017, 2019; Liu et al. 2018a). But what role does episodic accretion play in the formation of high mass stars? Because massive protostars form in deeply-embedded, compact protoclusters located at kiloparsec distances, interferometers with sub-arcsecond resolution like the SMA are essential for measuring changes in the luminosity of individual cluster members. As a result, the combination of SMA and ALMA has played a key role in the first detections of accretion outbursts in these more massive objects. The first two events both happened in early 2015, in opposite directions in the Milky Way. In parallel with an outburst seen in the infrared (Caratti o Garatti et al. 2017), S255IR-NIRS3 exhibited a factor of 2 increase in millimeter continuum emission that lasted for 2 years (Liu et al. 2018b). A larger and longer outburst occurred in NGC6334I-MM1, which increased in millimeter continuum flux density by a factor of 4 (Hunter et al. 2017a,b) with no signs of any decrease in ongoing monitoring at ALMA. Previously undetected at 18 microns (De Buizer et al. 2000), NGC6334I-MM1 is now the brightest object in the cluster in SOFIA images from 24-53 microns and the current spectral energy distribution of MM1 indicates a bolometric luminosity of ~10^5 $L_\odot$ (Hunter et al. 2019).

A distinctive feature of both of these massive protostellar outbursts is that they were heralded by strong flaring of their 6.7 GHz Class II methanol maser emission (Fujisawa et al. 2016, Szymczak et al. 2018, MacLeod et al. 2018), a phenomenon that is known to trace actively-accreting massive protostars (Cyganowski et al. 2009). In the case of NGC6334I-MM1, the maser flaring arose from the hot core MM1, which had never before shown such maser emission in 30 years of occasional interferometric imaging (Hunter et al. 2018). Its new emission continues to this day at essentially constant strength. During the Sardinia IAU meeting on masers in 2017, the presentation of these two impressive discoveries inspired the formation of an international maser monitoring collaboration called M2O (masermonitoring.org), whose goal is to identify new flares and to pursue follow up studies at infrared through radio wavelengths.

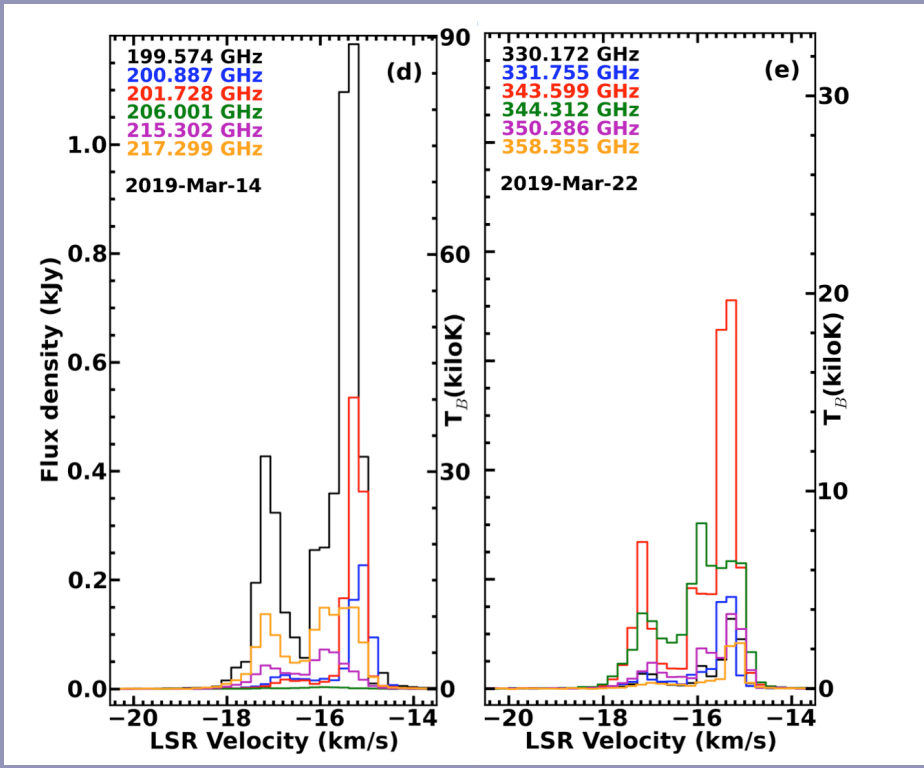

Figure 1: Integrated spectra from the SMA image cubes of 12 of the new methanol maser lines observed in very-extended configuration in March 2019 (excerpted from Brogan et al. 2019). Note the y-axis units of kiloJansky and kiloKelvin.

In mid-January 2019, the maser research group at the Ibaraki Station in Japan alerted their fellow M2O members of a 6.7 GHz methanol maser flare observed with the Hitachi 32m telescope toward an obscure massive star forming region G358.93-0.93 (Sugiyama et al. 2019). A spectral movie of the flare can be seen at: http://vlbi.sci.ibaraki.ac.jp/iMet/G358.9-00-190114/. With no prior observations in the SMA nor ALMA archives, very little was known about this protocluster aside from a luminosity estimate of 5700-22000 $L_{\odot}$ (Brogan et al. 2019), based on its detection in the (sub)millimeter and far-infrared surveys of ATLASGAL (Schuller et al. 2009), BGPS (Rosolowsky et al. 2010) and Herschel HiGAL (Molinari et al. 2016), along with an uncertain kinematic distance estimate of $6.75^{+0.37}_{-0.68}$ kpc. Unfortunately, at the time of discovery both ALMA and SMA were in their most compact configurations, which are not well suited to resolving a cluster at this large distance. Nevertheless, we pursued an SMA filler track to measure the dust continuum emission at the earliest possible time in hopes of catching an outburst on the rising side of its light curve for the first time.

While a continuum point source was easily detected in the first filler observation during daytime on Feb 6, the broad band spectrum recorded by the SWARM correlator in the 230 GHz band was quite odd-looking with a number of strong lines at frequencies unfamiliar to experienced observers of such regions, the brightest of which was at 199.574 GHz. After consulting the line catalogs (collated at http://splatalogue.net), it became apparent that all of the strong features corresponded to methanol lines, most of which were from torsionally-excited states with energies up to hundreds of Kelvin above the ground state. These intriguing SMA detections were reported to the M2O group and quickly led to the subsequent detection of eight additional new centimeter methanol maser lines in early March at telescopes in Australia (Breen et al. 2019) and South Africa (MacLeod et al. 2019), including three more torsionally-excited lines. It is important to recognize that the discovery of all of these new lines can trace their origin to the wideband nature of the SWARM correlator, a property which promotes serendipity.

Meanwhile, multi-epoch VLBI observations of the 6.7 GHz maser on February 2 and February 28 had been acquired at the Australian Long Baseline Array (LBA), which allowed the M2O group to trace the change in location of the maser excitation as the radiative outburst, or "heat wave", advanced through the circum-protostellar material (Burns et al. 2020). The SMA was scheduled to move to very extended configuration in early March, and we were fortunately granted DDT time to pursue this outburst at sub-arcsecond resolution. Observations on March 14 quickly confirmed that the new methanol lines were indeed maser transitions with peak brightness temperatures approaching 100,000 K, and in some cases triggering spike detection in the correlator software. A total of 13 maser lines were detected in the 230 and 345 GHz bands, including one line from the second torsionally excited state (v_t=2) at 330.172 GHz (Figure 1). On the same day, the first detection of $^{13}CH_3OH$ maser emission in the ISM was made in

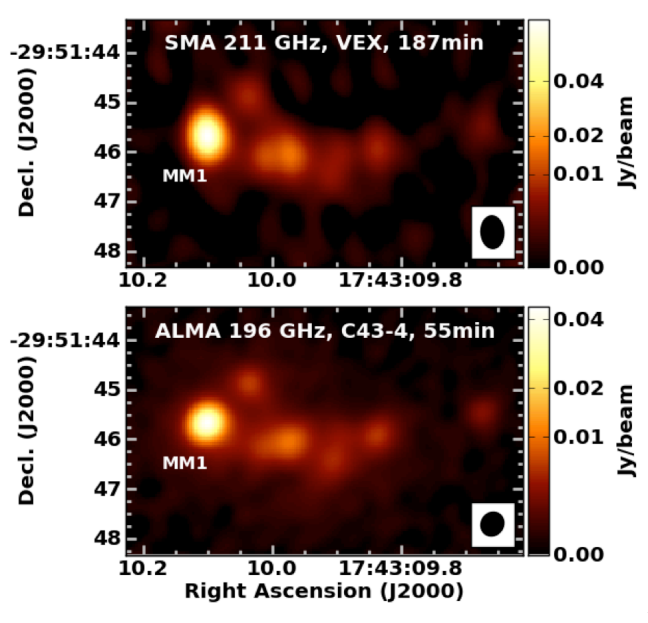

Figure 2 a: (Top panel) SMA continuum image observed on March 14, 2019 (0.66'' x 0.46'' synthesized beam, made with robust weighting = +0.5). **b:** (Bottom panel) ALMA Band 5 continuum image observed on April 16, 2019 with only 1.34 GHz of aggregate bandwidth (0.50" x 0.45" synthesized beam, made with robust weighting = 0.0). The new masers are located towards MM1.

this object in two lines at 14.300 and 14.782 GHz at the 65m Tianma Radio Telescope (TMRT) in China (Chen et al. 2019).

Once the astonishment of the new maser discoveries had been absorbed, we set to work on understanding the environment of the outburst by imaging the thermal emission dust and molecular gas (Brogan et al. 2019). The SMA continuum image revealed a protocluster of 8 sources (Figure 2a), with the maser emission arising from a compact ring of spots centered on the brightest component, MM1. However, the SMA spectra showed very few thermally-excited molecular lines, owing to the large distance to the source. To gain further spectral sensitivity, we submitted an ALMA DDT proposal for multi-band, multi-configuration follow-up. The first observation was taken a month later in configuration C43-4 in Bands 5, 6 and 7. The Band 5 observation had similar resolution to the SMA very-extended data but with much greater sensitivity (Figure 2b). Both MM1 and MM3 exhibit hot core spectra, with MM1 being the richer of the two. Their continuum spectral indices measured across the three bands was 3.06+-0.13 and 3.67+-0.17, consistent with dust emission, as expected for hot cores. The Band 6 observation also confirmed a fourteenth new maser line at 229.589 GHz. All of the masers had dropped in strength between the March SMA and April ALMA observations, by factors of 3-7. By the time of our next SMA observation on June 2, 2019, only the 217.299 GHz maser line remained detectable, and this v_t=1 line was still detectable in the most recent ALMA observation in July and October 2019. High-resolution ALMA images with a 200 au beam confirm that the torsionally-excited masers arise from numerous spots in a ring of diameter 2000 au (Brogan et al., in preparation).

Maser emission will arise from locations where the physical conditions are favorable for the maser pumping mechanism, and the line-of-sight affords a velocity-coherent high column density path length. The rapid evolution of the maser flare in G358.93−0.03, with dramatic changes over the course of only 1 month, together with the large spatial scale over which changes have occurred, require that the impetus for change must be radiative because the timescale for physical movement or bulk changes in the line-of-sight path is far too long.

One explanation for the maser flare is an abrupt change to more favorable physical conditions, such as the rapid heating of dust that occurs in a protostellar accretion event (Johnstone et al. 2013). Comparing our measurement of the 0.87 mm ATLASGAL flux density (1.11 Jy) with the total ALMA 0.89 mm measurement after scaling to 0.87 mm, 1.22±0.04 Jy (using the flux-weighted mean dust spectral index of +3.3), yields a post-flare excess of 0.11±0.19 Jy at 0.87 mm, which is consistent with no change. It is also feasible that a modest brightening of MM1, which currently represents only 25% of the total ALMA flux density, is being masked by a commensurate loss in the total flux of the protocluster due to spatial filtering of larger-scale emission by ALMA compared to ATLASGAL's 19'' beam. Unfortunately, the lack of prior higher resolution millimeter data prevents us from testing this possibility. In any case, the two post-flare (sub)millimeter observations (March and April) do not show evidence for any significant (>10%) change in the continuum flux of MM1 (Figure 2).

In summary, the uncertainty in the pre- and post-flare submillimeter continuum flux densities of G358.93-0.03 allow for a modest (10%) brightening to have occurred. Because this upper limit originates from the Rayleigh-Jean side of the dust spectrum, we cannot rule out modest changes in total dust luminosity (up to ~50%). But the luminosity appears to have remained steady between 2 and 3 months after the flare began, in contrast to the maser lines themselves. Alternatively, because the heating and cooling timescale of the dust is shorter than the gas (Johnstone et al. 2013), it is possible that the heating event was quite brief (<2 months), and had already subsided before our March SMA observation, with the excited masers steadily decaying during the subsequent weeks. In contrast, the (sub)millimeter emission of S255IR-NIRS3 increased by a factor of 2 and lasted for 2 years (Liu et al. 2018b), while NGC6334I-MM1 increased by a factor of 4 and

has yet to subside after 4 years (Hunter et al. 2017a,b). Thus, the first three outbursts identified in massive protostars have all shown distinctly different temporal behavior and magnitude. This result suggests an underlying physical structure that promotes stochastic changes in accretion rate, of variable magnitude, consistent with the results of recent hydrodynamical models of accretion-driven bursts which arise due to azimuthal asymmetries in the accretion flow (Meyer et al. 2017). The brief, unprecedented flaring of torsionally-excited methanol masers in G358.93-0.03 may have occurred in the other two objects but was simply missed out of ignorance, or it may be the result of a rare geometry or viewing angle. To test the latter possibility, in ALMA Cycle 7 we are imaging numerous outflow tracers in G358.93-0.03 with high spatial dynamic range. In the meantime, the identification and follow-up study of future outbursts by M2O in other similar objects will hopefully provide further critical information on the accretion mechanism of massive protostars.

REFERENCES

- Breen, S., S. L., Sobolev, A. M., Kaczmarek, J. F., et al. 2019, ApJL, 876, L25
- Brogan, C.L., Hunter, T.R., Towner, A.P.M., et al. 2019, ApJL, 881, L39
- Burns, R. A., et al, 2020, Nature Astronomy, in press
- Caratti o Garatti, A., Stecklum, B., Garcia Lopez, R., et al. 2017, Nature Physics, 13, 276
- Chen, X., Sobolev, A.M., Breen, S., et al, 2019, Nature Communi cations, submitted
- Cyganowski, C. J., Brogan, C. L., Hunter, T. R., Churchwell, E. 2009, ApJ, 702, 1615
- De Buizer, J. M., Pina, R. K., & Telesco, C. M. 2000, ApJS, 130, 437
- Evans, N.J., Dunham, M.M., Jørgensen, J.K., et al. 2009, ApJS, 181, 321
- Frimann, S., Jørgensen, J, Dunham, M., et al. 2017, A&A, 502, 120
- Frimann, S., Jørgensen, J, Dunham, M., et al. 2018, SMA Newsletter 25
- Fujisawa, K., Yonekura, Y., Sugiyama, K., et al. 2015, ATel, 8286
- Hartmann, L., Herczeg, G., & Calvet, N. 2016, ARA&A, 54, 135
- Hunter, T. R., Brogan, C. L., MacLeod, G., et al. 2017a, ApJL, 837, 29
- Hunter, T. R., Brogan, C. L., MacLeod, G., et al. 2017b, SMA Newsletter, 24
- Hunter, T.R., Brogan, C. L., MacLeod, G.C., et al. 2018, ApJ, 854, 170
- Hunter, T. R., Brogan, C. L., et al. 2019, ALMA science conference, Cagliari, Italy
- Johnstone, D., Hendricks, B., Herczeg, G.J., et al. 2013, ApJ, 765, 133
- Kenyon, S.J., Hartmann, L.W., Strom, K.M., et al. 1990, AJ, 99, 869
- Liu, H. B, Dunham, M., Pascucci, I. et al., 2018a, A&A, 612, 54
- Liu, S.-Y., Su, Y.-N., Zinchenko, I., et al. 2018b, ApJL, 863, 12
- MacLeod, G. C., Smits, D., Goedhart, S., Hunter, T.R. et al., 2018, MNRAS, 478, 1077
- MacLeod, G. C., Sugiyama, K., Hunter, T. R., et al. 2019, MNRAS, 489, 3981
- Meyer, D.M.-A., Vorobyov, E.I., Kuiper, R., & Kley, W. 2017, MNRAS, 464, 90
- Molinari, S., Schisano, E., Elia, D., et al. 2016, A&A, 591, A149
- Offner, S.S.R., & McKee, C.F. 2011, ApJ, 736, 53
- Rosolowsky, E. Dunham, M. K., Ginsburg, A., et al. 2010, ApJS, 188, 123
- Schuller, F., Menten, K. M., Contreras, Y., et al. 2009, A&A, 504, 415
- Sugiyama, K., Saito, Y., Yonekura, Y., & Momose, M. 2019, ATel, 12446
- Szymczak, M., Olech, M., Wolak, P., G´erard, E., & Bartkiewicz, A. 2018, A&A, 617, A80

HARO 2: OUTFLOWING MOLECULAR GAS AROUND A HOT SUPERBUBBLE IN A NEARBY LYα GALAXY

Sara Beck (Tel Aviv University), Pei-Ying Hsieh (ASIAA), and Jean Turner (UCLA)

Molecular gas is the fuel of star formation. Accretion of molecular gas by a galaxy can trigger a burst of formation of hot and energetic young stars; feedback from the young stars can then expel and disperse the remaining molecular gas. An excellent laboratory for study of this gas-star cycle is the nearby (~20 Mpc) dwarf galaxy Haro 2 (Mkn 33, Arp 233). Haro 2 holds a ~6 Myr old starburst which has created super-star clusters and drives multiple ionized gas outflows including a hot X-ray superbubble (Summers et al 2001), a kpc-wide system of Hα filaments and shells (Mendez & Estaban 2000), and strong Lyα emission with a P Cygni profile (Lequeux et al 1995).

Observations of CO(1-0) line with moderate (3.3'') spatial resolution by Bravo-Alfaro et al. (2004) found a strong velocity gradient in the molecular gas at an angle of ~50 degrees to the photometric axis of the galaxy, which they suggested traces the accretion event that triggered the starburst. We observed the CO(2-1) line emission of Haro 2 with the SMA with the extended and compact configurations and combined the

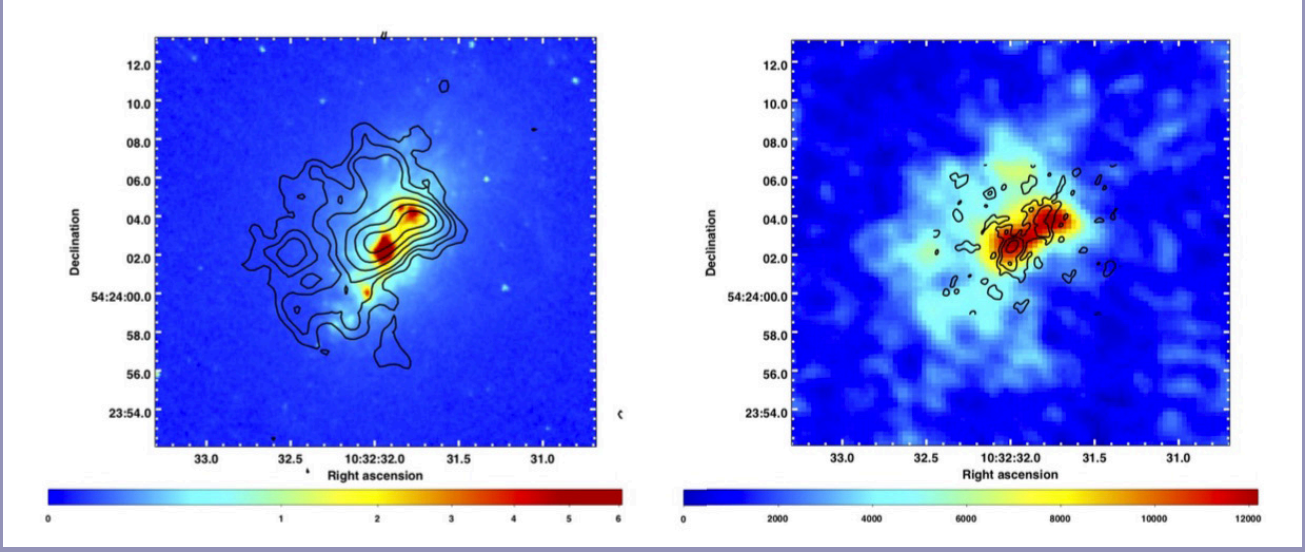

Figure 1: Left: the intergrated CO(2-1) line flux of Haro 2 in contours (contour unit = 9730, base =11020 Jy/bm (m/s)) over the Hα emission measured by HST in colors. Right: the integrated CO(2-1) line flux in color and the 6 cm radio continuum from the VLA archives in contours; contour unit is 0.26 mJy/bm and the base 0.17 mJy/bm.

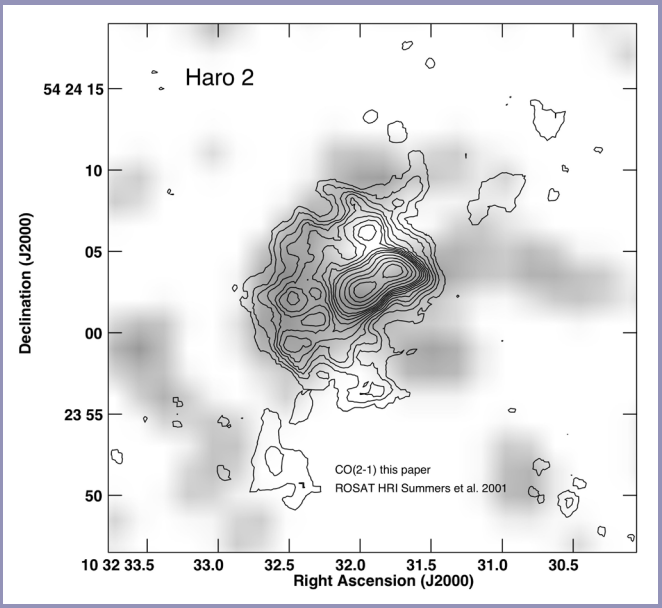

Figure 2: CO(2-1) integrated emission in contours (levels are multiples of 600mJy/bm km/s up to n=10 and 1200mJy/bm km/s for n>10) superimposed on the X-ray emission imaged by Summers et al 2001 with HRI on ROSAT. The X-ray emission forms a superbubble coincident with the extended component of CO(2-1).

data to create images with spatial resolution 1.96 × 1.6'' and 4.2 km/s velocity resolution, a significant improvement over the earlier results.

Figure 1 shows the spatial distribution of the molecular gas, the Hα emission and thermal radio continuum. The Hα and radio emission show the clumps of young star clusters in the starburst; the clumps lie roughly in a line along the photometric axis of the galaxy. There is strong CO(2-1) emission on the starburst, as expected, but there is also extended emission over more than 1 kpc east and north of the main optical body of the galaxy. This extended component was not apparent in the earlier CO(1-0) maps because they had lower resolution and sensitivity. Figure 2 shows the molecular gas and the soft X-ray emission measured by Summers (2001) and demonstrates that the CO emission east of the main galaxy coincides spatially with the X-ray bubble.

The extended component is distinctive kinematically as well spatially, as shown in Figure 3. That figure displays separately the integrated line emission from velocities blue and red of 14580 km/s. The starburst is at red velocities and the extended emission at blue, with little overlap. The red velocities plotted include those expected from the rotation of the galaxy; the blue velocities are out of that range.

Comparing Figure 3 to the result of Bravo-Alfaro et al we see that they did not detect all the extended emission but only the brightest region, which created an apparent velocity gradient at angles to the galaxy and 'twisted axes' in their first moment map. The SMA velocity channel maps in Figure 4 show instead a velocity gradient along the line of star clusters consistent with simple galactic rotation.

The blue extended emission appears to be associated with the hot gas in the X-ray bubble, not with the body of the galaxy and its kinematics must be considered independantly. The channel maps of Figure 4 show that the blue extended emission has two velocity peaks separated by ~70 km/s .

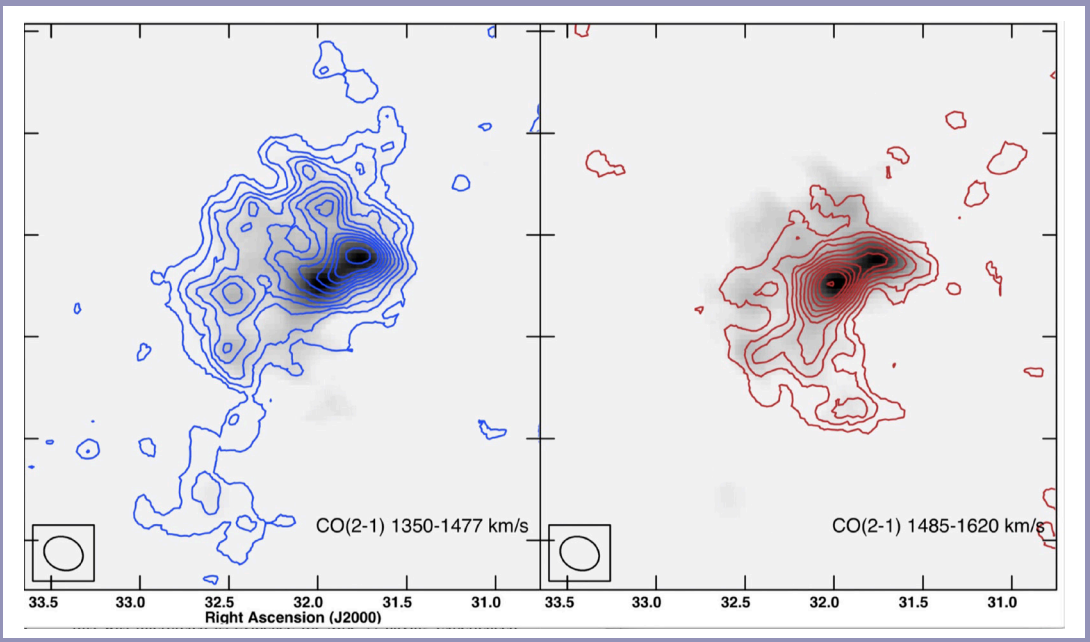

Figure 3: Intergrated CO(2-1) line emission over the blue (left) and red (right) velocity ranges. The velocities included in each image are shown in the lower right and the beam size in the lower left. Contours are the same as in previous figure.

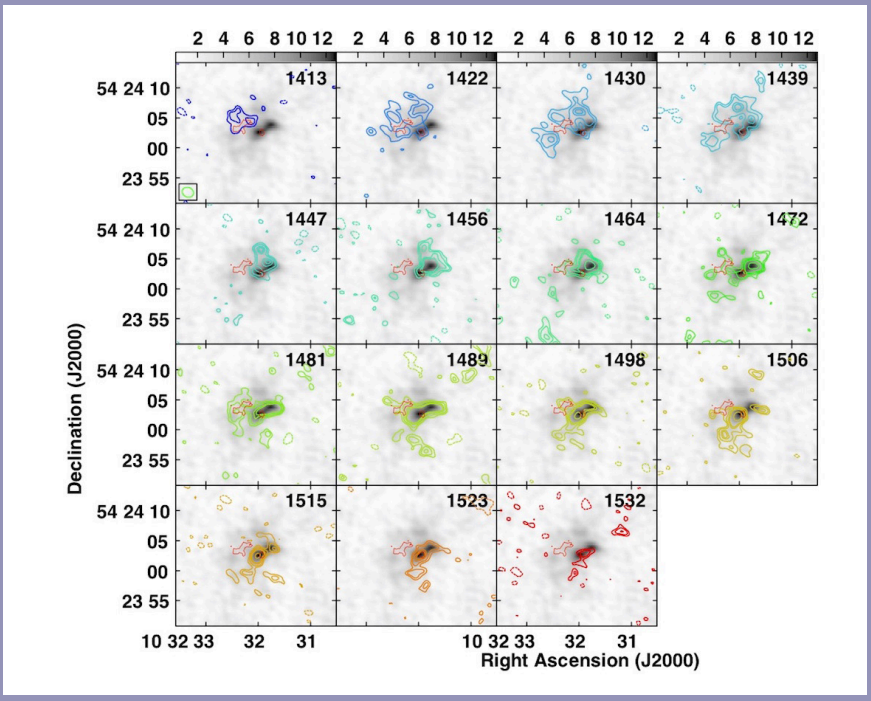

Figure 4: Velocity channel maps of the CO(2-1) line in Haro 2. Each channel is 4.2 km/s and the central velocity is shown in each panel. The roughly trapezoidal red shape in each panel is the region of highest velocity dispersion.

This is the kinematic signature of an expanding bubble, shell or cone. It could also arise in overlapping outflows from several clusters; that the two velocity peaks are slightly offset in space (see the figure) may support this model. We suggest that the young star clusters are driving a large-scale outflow, which has also created the X-ray superbubble, and that the blue CO(2-1) emission arises in the molecular gas entrained in the outflow.

Haro 2 is the first dwarf galaxy known where outflowing molecular gas is associated with a X-ray bubble. It is likely that there are other such sources in the nearby universe, as dwarf galaxies often drive strong winds. The history of observations of Haro 2 shows how the kinematic signatures of outflows can be missed or misinterpreted at low spatial resolution. The high resolution and sensitivity of the SMA were crucial in discovering the true nature of the Haro 2 activity and we expect the SMA to be important in further searches for molecular gas outflows from dwarf galaxies. This paper will appear in MNRAS.

REFERENCES

- Bravo-Alfaro, H., Brinks, E., Baker, A. J., Walter, F., & Kunth, D. 2004, AJ, 127, 264
- Lequeux, J., Kunth, D., Mas-Hesse, J. M., & Sargent, W. L. W. 1995, A&A, 301, 18
- Mendez, D. I., & Esteban, C. 2000, A&A, 359, 493
- Summers, L. K., Stevens, I. R., & Strickland, D. K. 2001, MNRAS, 327, 385

FORMATION OF MASSIVE PROTOSTELLAR CLUSTERS – OBSERVATIONS OF MASSIVE 70 μm DARK MOLECULAR CLOUDS

Shanghuo Li (SHAO), Qizhou Zhang (CfA), Thushara Pillai (BU), Ian W. Stephens (CfA), Junzhi Wang (SHAO) and Fei Li (SHAO)

The feedback of massive stars and stellar clusters, such as radiation, wind, and supernovae, accounts for most of the energy budget in galaxies. However, our understanding of massive star and cluster formation is still poor (Zinnecker & Yorke 2007; Motte et al. 2018). The physical and chemical conditions of clouds at early phases of evolution are crucial for unraveling the mystery of massive star and cluster formation. Massive (>10^2 $M_\odot$) and dense (>10^3 cm^{-3}) molecular clumps that are lack of signs of ongoing star formation activities are considered the prime candidates for such studies (Carey et al. 1998; Rathborne et al. 2006; Wang et al. 2006; Henning et al. 2010; Ragan et al. 2012).

Infrared dark clouds (IRDCs) consist of cold and dense gas and dust at the early stages of evolution prior to the star formation activities significantly altering the physical conditions of the natal cloud (Carey et al. 1998; Rathborne et al. 2006; Ragan et al. 2012, and references therein). In particular, massive molecular clouds who are dark in the infrared wavelengths up to 70 μm (Rathborne et al. 2006; Wang et al. 2006) provide ideal laboratories to investigate the initial condition of massive star and cluster formation (Dunham et al. 2008; Ragan et al. 2012; Stutz et al. 2013; Elia et al. 2017).

To study the processes of massive star and cluster formation within massive clumps, we used the Submillimeter Array (SMA, Ho et al. 2004) to observe a sample of seven high-mass 70 μm dark clumps (Figure 1). Using the 1.3 mm continuum emission, we have identified a total of 44 cores in 7 clumps, with gas masses ranging from 1.4 to 77.1 $M_\odot$. Twenty-nine dense cores have masses greater than 8 $M_\odot$ and the other fifteen dense cores have masses between 1.4 and 7.5 $M_\odot$. To study the physical structure of identified cores, we estimated core density distributions using the 1.3 mm continuum data. Assuming that the core density follows a power-law relation with radius as $\rho \propto r^{-b}$, we found the index b to be between 0.6 and 2.1 with a mean value of 1.3. Our results are in agreement with previous investigations, as we find no significant differences between power-law indexes of our 70 μm dark dense cores and the above mentioned high- and low-mass objects (see van der Tak et al. 2000; Mueller et al. 2002; Beuther et al. 2005; Butler & Tan 2012; Motte & André 2001; Tobin et al. 2015; Shirley et al. 2002).

Protostellar outflows as revealed by the CO emission are detected toward 17 out of 44 identified dense cores. This indicates that these 70 μm dark clumps have embedded protostars, and many dense cores are protostellar in nature (see also Pillai et al. 2019). Some dense cores are associated with faint or no line emission (e.g., CO/^{13}CO/C^{18}O, CH_3OH, H_2CO, HCN and HCO^+), and could be starless or prestellar candidates. With the molecular line emission, we found signs of chemical differentiation among different dense cores within the same parent clumps, which suggests that they maybe at different evolutionary stages.

High-velocity CO emission is detected in all of the clumps, except for AGAL030. The maximum velocities ($|v - v_{lsr}|$) for

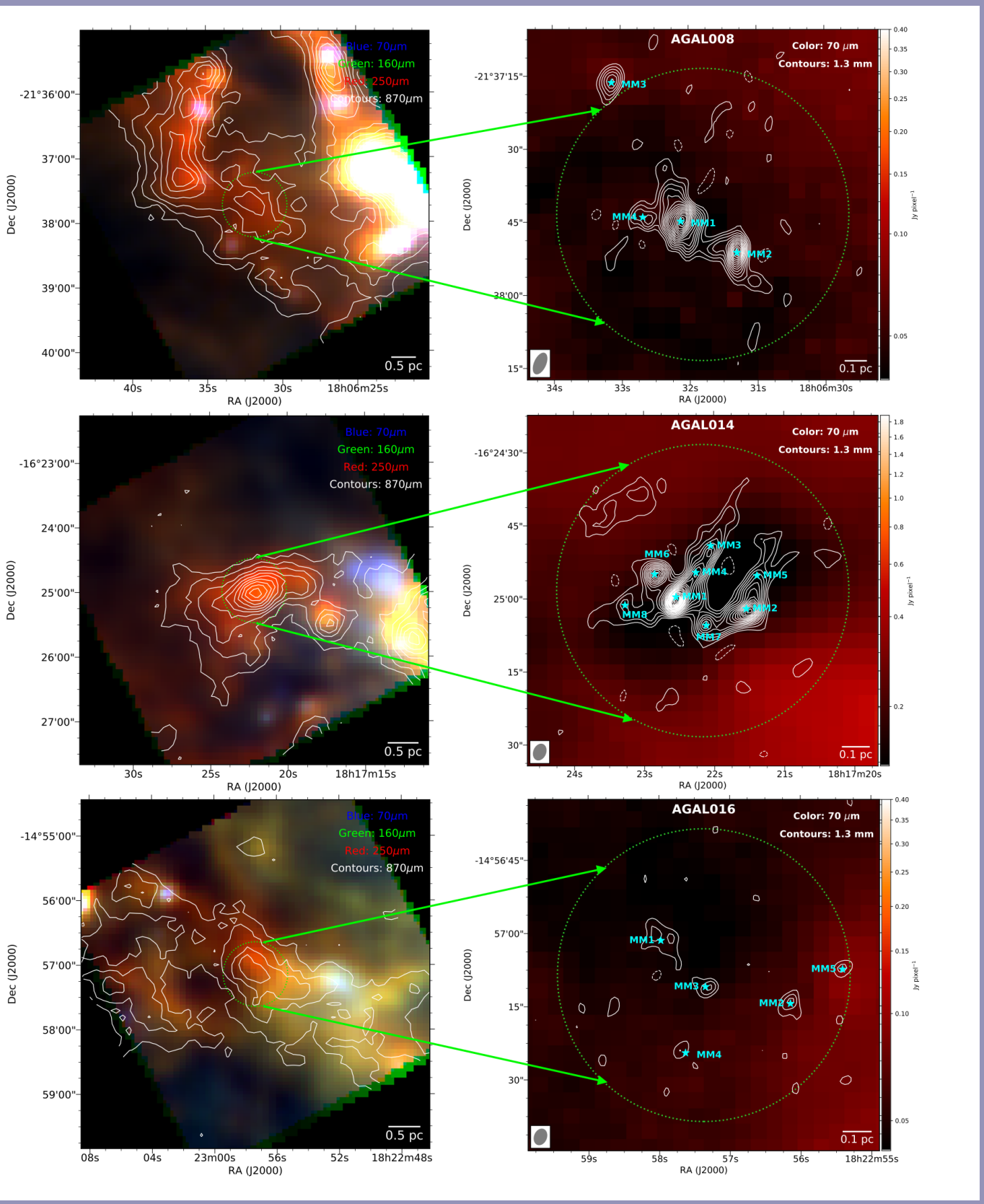

Figure 1: Left: the APEX 870 μm emission (white contours) overlaid on three-color Herschel composite image (blue/green/red = 70/160/250 μm). The white contours are at levels of ±(4, 8, 12 ....)× σ, where the σ is the rms level for each source. Right: the 1.3 mm dust continuum emission obtained from the SMA overlaid on Herschel 70 μm image. The white contours are at levels of ±(3, 5, 7, 9 ....)× σ. The dash circle is the SMA primary beam FWHM size. The synthesized beam is shown in the bottom-left corner of the image.

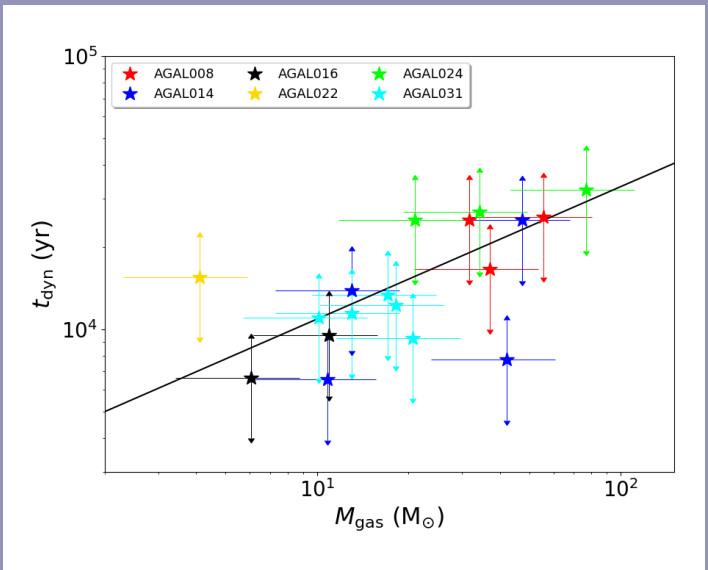

Figure 2 Dense core mass versus outflow dynamical timescale. The correlation coefficient is about 0.62 from the Spearman-rank correlation test. The black solid line is the best least-squares fitting result y = $3570x^{0.5}$. The errorbar of t_{dyn} corresponds to the mean inclination angle ([[θ]] ≈ 57.3°) correction. The errorbar of M_{gas} corresponds to its measurement uncertainty.

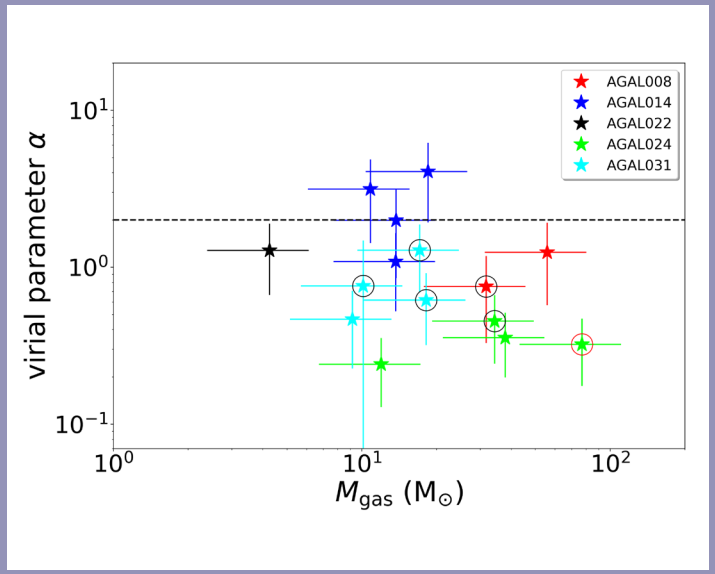

Figure 3 The virial parameter α, defined as the ratio between the virial mass and gas mass, against gas mass of dense cores. The red and black circles represent cores associated with high- (velocity >= 30 km s^{-1} with respect to the source systemic velocity) and low-velocity (velocity < 30 km s^{-1}) CO outflows, respectively.

the CO outflow emission range from 5 to up to 56 km s^{-1} with respect to the source systemic velocity. There are five dense cores associated with high velocity CO outflow emission ($|v - v_{lsr}|$ >= 30 km s^{-1}) within a small spatial scale of <= 0.22 pc, while the rest of the dense cores are associated with low-velocity CO outflows ($|v - v_{lsr}|$ < 30 km s^{-1}). These results suggest that these 70 μm dark clumps host protostars, and therefore they are not quiescent in star formation.

We find a positive correlation between the outflow dynamical timescale and the gas mass of dense cores (Figure 2), with a correlation coefficient of 0.62 estimated from the Spearman-rank correlation test. Massive cores tend to have a longer outflow dynamical timescale than that of less massive cores. This trend suggests that the more massive cores have a longer accretion history that allows them to assemble more materials. This relation also implies that the most massive cores may form earlier than the less massive cores. A confirmation of this trend from a more sensitive and larger sample is still needed.

A thermodynamic analysis found that the dense cores are not in a virial equilibrium. The derived virial parameters of dense cores range from 0.2 to 4.1 with a mean value of 1.1 (Figure 3). This indicates that most of the dense cores are gravitationally bound. We found no significant difference in virial parameters for dense cores associated with and without CO outflows. Figure 4 shows the virial parameters versus the gas mass of dense cores. We note that the most massive cores tend to have lower virial parameters.

A fragmentation analysis finds that the gas masses of identified low-mass dense cores are roughly consistent with the pure thermal Jeans fragmentation, while massive cores are approximately consistent with the turbulent Jean fragmentation (Figure 4). Comparisons of fragments with the clump properties (column and volume densities, Mach number, gas mass, virial parameter and density distribution) show no apparent correlation. This could be due to either the small sample size, or the fact that fragmentation is afected by a combination of multiple physical processes (e.g., turbulence, magnetic fields, protostar feedback, and density distributions).

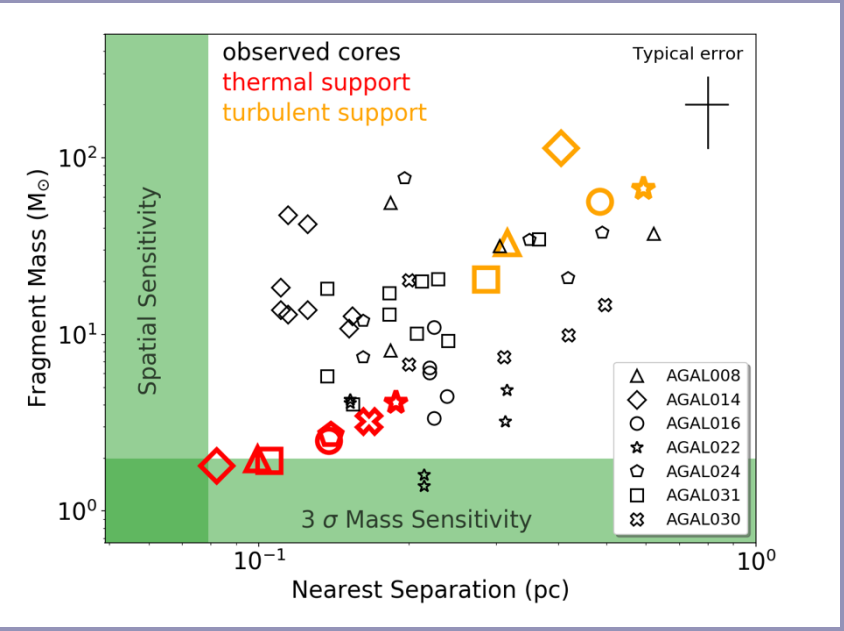

Figure 6: Fragment mass versus projected separation on the sky of the nearest neighbor fragments. The black symbols are the fragments identified by SMA observations. The black cross is the typical uncertainly of the observed fragments. The red symbols represent the prediction of thermal Jeans fragmentation. The orange symbols represent the prediction of turbulent Jeans fragmentation, where the turbulent component is from the clump non-thermal NH_3 line width. The green shaded regions show the mass sensitivity and spatial resolution limit of the observations.

REFERENCES

- Beuther, H., Schilke, P., Menten, K. M., et al. 2005, ApJ, 633, 535
- Butler, M. J., & Tan, J. C. 2012, ApJ, 754, 5
- Carey, S. J., Clark, F. O., Egan, M. P., et al. 1998, ApJ, 508, 721
- Dunham, M. M., Crapsi, A., Evans, Neal J., I., et al. 2008, ApJS, 179, 249
- Elia, D., Molinari, S., Schisano, E., et al. 2017, MNRAS, 471, 100
- Henning, T., Linz, H., Krause, O., et al. 2010, A&A, 518, L95
- Ho, P. T. P., Moran, J. M., & Lo, K. Y. 2004, ApJL, 616, L1
- Motte, F., & Andŕe, P. 2001, A&A, 365, 440
- Motte, F., Bontemps, S., & Louvet, F. 2018, ARA&A, 56, 41
- Mueller, K. E., Shirley, Y. L., Evans, II, N. J., & Jacobson, H. R. 2002, ApJS, 143, 469
- Pillai, T., Kauffmann, J., Zhang, Q., et al. 2019, A&A, 622, A54
- Ragan, S., Henning, T., Krause, O., et al. 2012, A&A, 547, A49
- Rathborne, J. M., Jackson, J. M., & Simon, R. 2006, ApJ, 641, 389
- Shirley, Y. L., Evans, Neal J., I., & Rawlings, J. M. C. 2002, ApJ, 575, 337
- Stutz, A. M., Tobin, J. J., Stanke, T., et al. 2013, ApJ, 767, 36
- Tobin, J. J., Stutz, A. M., Megeath, S. T., et al. 2015, ApJ, 798, 128
- van der Tak, F. F. S., van Dishoeck, E. F., Evans, II, N. J., & Blake, G. A. 2000, ApJ, 537, 283
- Wang, Y., Zhang, Q., Rathborne, J. M., Jackson, J., & Wu, Y. 2006, ApJL, 651, L125
- Zinnecker, H., & Yorke, H. W. 2007, Annual Review of Astronomy and Astrophysics, 45, 481

OPTICAL ALIGNMENT USING RASPBERRY PI CAMERAS

Lingzhen Zeng (CfA), Scott Paine (CfA), and Ramprasad Rao (ASIAA)

Accurate optical alignment is essential to achieving full performance from a telescope system. For the SMA, there is a further requirement that independent receivers have arc-second level co-pointing on sky for dual-band observations and single-band polarimetry. To help achieve and maintain this alignment performance, we designed and tested an optical alignment technique based on Raspberry Pi cameras mounted in a fixture made from a modified spare SMA optical insert. Measurement results show that with this alignment technology we can achieve sub-arcmin angular alignment accuracy of optical elements with corresponding demagnified impact on pointing of about one arcsecond.

Currently, the SMA employs receiver cartridges arranged in a ring in a single large cryostat. Above each receiver is an optics insert mounted on rails in a cylindrical cage above the cryostat. A rotating grid polarizer and mirror arrangement along the cryostat/optics cage axis is used to combine the beams from pairs of orthogonally-polarized receivers. The alignment fixture described here was developed to improve the SMA optics cage alignment.

The alignment fixture is substituted for a receiver's optics insert to verify and adjust the combiner grid and mirror. Figure 1 (a) shows a CAD model of the alignment fixture installed in an SMA optics cage. Two Raspberry Pi cameras (camera A and camera C) are mounted inside the fixture with their respective pointing directions perpendicular to the combiner mirror (45° mirror) and to a flat autocollimating mirror mounted on the back of the combiner grid frame. The distance from camera A to the combiner mirror is 306.3 mm and the distance from camera C to the grid's autocollimating mirror is 452.8 mm. For improved angular resolution, we replaced the 3.6 mm F/2.9 lenses supplied with the cameras with 25 mm F/1.2

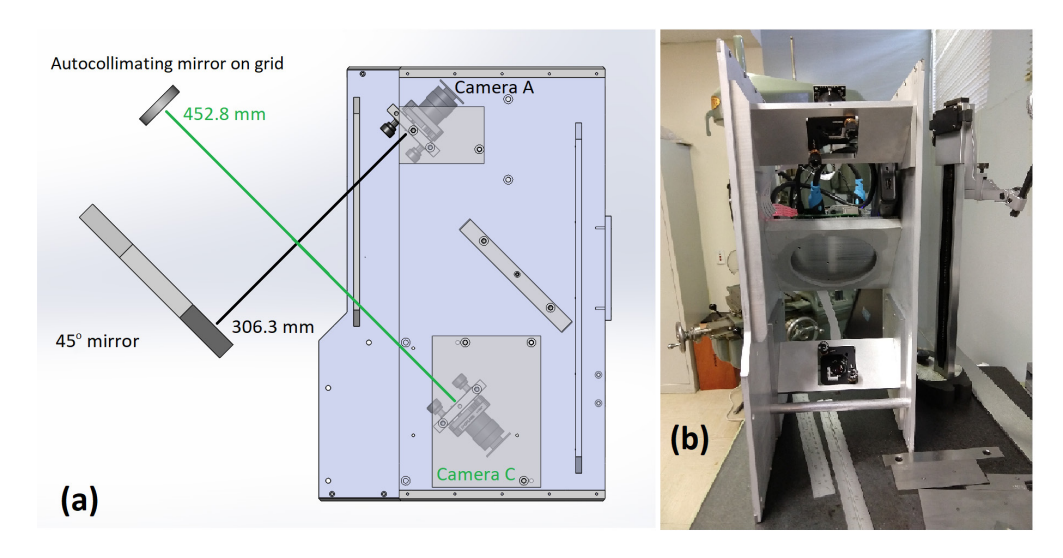

Figure 1: The CAD model and a photo showing the front view of the alignment fixture.

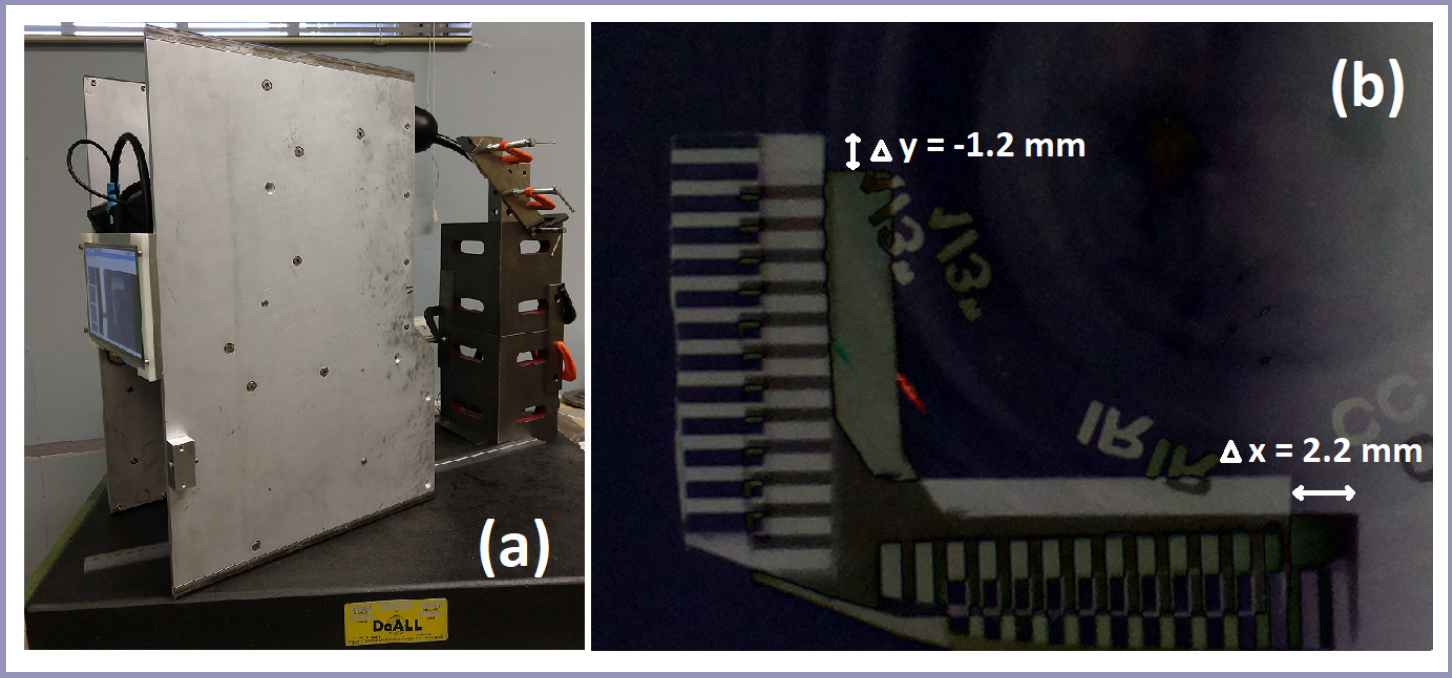

Figure 2: Alignment fixture under calibration and a sample image showing the measurement result of a combiner mirror in one of SMA optics cage.

lenses. In principle, still higher angular precision could be achieved using telephoto lenses, but the absolute alignment accuracy is ultimately limited by the fixture's own calibration accuracy. Figure 1 (b) shows a photo of the cameras with two orthogonal line scales mounted close to the lenses for x- and y- direction offset measurement in autocollimation. Each line scale has a resolution of 1.0 mm per line. The cameras take reference images of the line scales as reflected in standard calibration mirrors, for later comparison with measurement images reflected in the mirrors to be aligned. By stacking the reference and measurement images, we can read off the x- and y- linear offsets between them to about 1/5 of a scale line. Based on the distances from the cameras to the mirrors, these linear image offsets are converted into the corresponding angular alignment offsets.

The optical alignment fixture was designed and built as a self-contained high-precision device. The overall assembly tolerance is within 1.0 mil (25.4 μm) measured at the four corners of the fixture. The cameras are controlled by a Raspberry Pi computer through a multi-camera adapter module. The computer can be operated through a 7-inch touchscreen monitor built into the fixture. The computer, monitor and cameras are powered by an external battery pack, which can power the alignment fixture for several days after a full charge.

The alignment fixture is calibrated on a flat granite surface plate, using precision angle blocks and parallels. As shown in figure 2 (a), the polished surface of a 45° angle block is used as a standard calibration mirror and placed perpendicular to the cameras at the distances shown in figure 1 (a) for mirror alignment. Reference images are then acquired of the line scales next to each camera as seen in reflection off the angle block. The tolerance of the calibration is about 0.1 mm of linear offset in both x- direction and y- direction, corresponding to an angular offset of about 0.5′ for the combiner and 0.4′ for the grid. The calibration was performed in the SMA laboratory in Cambridge and repeated in Hilo to verify that it was unaffected by shipping.

In the field, the alignment fixture takes images in the antenna optics cages and overlays them on the reference images to reveal the offsets in x- and y- directions. Figure 2 (b) shows an example of an image in reflection off a combiner mirror, which has linear x-offset = + 2.2 mm and y-offset = - 1.2 mm, corresponding to angular offsets of 12.3' and 6.7'. Using the sensitivities derived in [1], we can convert them into system sky offsets of + 2.5″ in x- direction and - 1.3″ in y- direction, where x- is the θ and y- is the ρ direction of the cryostat, respectively. Using this alignment fixture, we checked the alignments of the combiner mirror and grid for all eight antennas. Most of the y-offsets, which relate to dead-reckoned assemblies not intended to be adjusted, were found to correspond to sky offsets less than 1 arcsecond. The x-offsets, which depend on correct encoder positions being assigned to each receiver selection position, were typically larger. New nominal positions were calculated based on the x- offsets and the

corresponding corrections have been made in SMA configuration data, to support arcsecond-level on-sky pointing.

In conclusion, we find that compact, low-cost cameras such as the Raspberry Pi cameras employed here can be used to construct simple and effective metrology fixtures for setting and maintaining optical alignment of radio telescope systems.

REFERENCES

- Paul K. Grimes, Scott N. Paine, Ramprasad Rao, Tirupati K. Sridharan and Lingzhen Zeng, "Tolerancing of the Submillimeter Array Optics using Physical Optics Simulations", 29th IEEE International Symposium on Space THz Technology (ISSTT2018), Pasadena, CA, USA, March 26-28, 2018.

RTDC UPDATE

The SMA public archive has expanded its capabilities. It is now possible to search over multiple source names or sets of coordinates, where the coordinate search allows each pair to have its own search radius. The results table now includes a 'supplemental plot' column linking to a pdf of phase rms, system temperature, opacity and weather conditions. There is also the ability to show/hide columns in the results table.

Website: www.cfa.harvard.edu/cgi-bin/sma/smaarch.pl

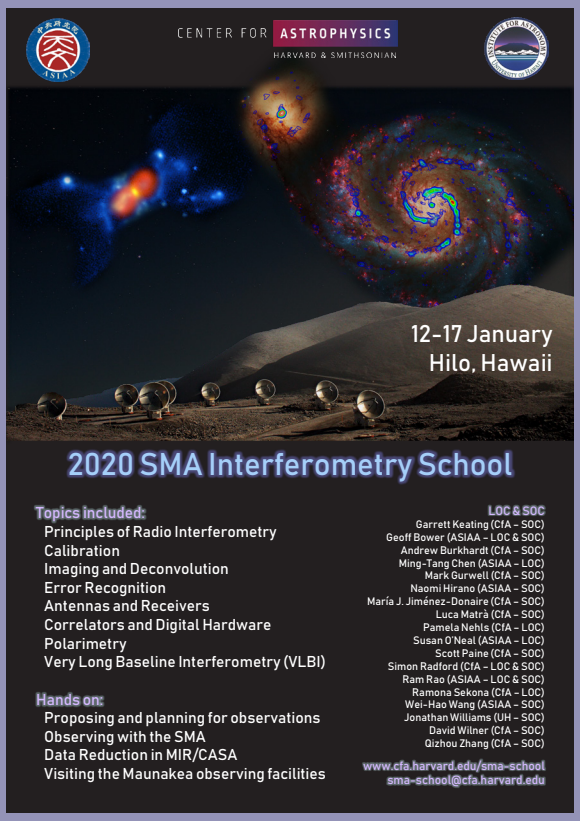

Ram Rao (left) showing the students the inner workings of the SMA antenna, and how the optics direct the light coming from the sky to the receivers in the cryostat below.

SMA INTERFEROMETRY SCHOOL 2020

The Center for Astrophysics, in conjunction with the Academia Sinica Institute of Astronomy and Astrophysics and the University of Hawaii, held the first Submillimeter Array Interferometry School from January 12 - 17, 2020. The school was conducted at the Hilo facilities of the Smithsonian Astrophysical Observatory and the University of Hawaii Institute for Astronomy.

The SMA Interferometry School aims to provide advanced undergraduates, graduate students, post-docs and scientists outside the field with a broad knowledge of interferometry and data reduction techniques at (sub)millimeter wavelengths. The students are trained through a mixture of lectures, hands-on demonstrations, and group training sessions and observing projects. Though the weather was formidable, including some significant snowfall on Maunakea, each of the student groups were able to collect data with the SMA on a wide variety of astronomical targets, from local star-forming regions to high-redshift galaxies.

The school hosted a total 20 students from 17 different institutions and 9 different countries. The lectures -- which were open to the astronomy community in Hilo at large -- were attended by more than 60 people. Presentations from the lecture component of the school can be found here:

https://www.cfa.harvard.edu/sma-school/program

The organizing committee wishes to thank all those who helped to put on the school, particularly the staff in Hilo, who helped provide a warm welcome to the students during their visit.

Those who are interested in participating in the SMA Interferometry School in the future are encouraged to contact **sma-school@cfa.harvard.edu** for further information.

SCIENCE WITH THE SUBMILLIMETER ARRAY: PRESENT AND FUTURE, NOVEMBER 4-5, 2019, ASIAA, TAIPEI

The workshop 'Science with the Submillimeter Array: Present and Future' was held on November 4 through 5, 2019, in the Academia Sinica Institute of Astronomy and Astrophysics in Taipei. Over 100 participants attended the workshop. The meeting featured oral and poster presentations that highlighted recent SMA results since the deployment of the SWARM correlator in 2017, discussed synergies with other facilities, and explored the science potential with the wSMA that offers four times more spectral bandwidth than the current SMA.

Oral presentations at this meeting can be found at the workshop website:
https://events.asiaa.sinica.edu.tw/workshop/20191104/program.php

Scientific Organizing Committee: Huei-Ru Vivien Chen (NTHU), Naomi Hirano (ASIAA), Patrick Koch (ASIAA; co-chair), Hau-Yu Baobab Liu (ASIAA), Scott Paine (CfA), David Wilner (CfA), Qizhou Zhang (CfA; co-chair)

CALL FOR STANDARD OBSERVING PROPOSALS - 2020A SEMESTER

We wish to draw your attention to the latest Call for Standard Observing Proposals for observations with the Submillimeter Array (SMA). This call is for the 2020A semester with observing period **16 May 2020 – 15 Nov 2020.**

Standard Observing Proposals

Submission deadline: **05 Mar 2020 21:00 UTC / 05 Mar 2020 16:00 EST / 06 Mar 2020 05:00 Taiwan**

Proposal Information and Submission **http://sma1.sma.hawaii.edu/proposing.html**

The SMA is a reconfigurable interferometric array of eight 6-m antennas on Maunakea jointly built and operated by the Smithsonian Astrophysical Observatory and the Academia Sinica Institute of Astronomy and Astrophysics. The array operates in the 230, 345 and 400 GHz bands, observing simultaneously with two orthogonally polarized receivers, one in the 230 GHz or 345 GHz band and the other in the 240 GHz or 400 GHz band (with full polarimetric observations available using the 230+240 or 345+400 band combinations).

The SMA configurations include antenna separations ranging between 9 m and 508 m. The small antennas allow access to low spatial frequencies (with projected baselines as short as 6-m) in the sub-compact configuration, and at the other extreme, the finest angular resolution with the very extended configuration at 345 GHz is ~ 0.25". The compact and extended configurations complete the range. The characteristics, performance and sky coverage of the SMA are both similar and complementary to those of the stand-alone Atacama Compact Array (ACA) component of ALMA, while providing full access to the northern sky.

The heart of the SMA backend is the SWARM correlator, able to process 8 GHz bandwidth (IF coverage of 4 to 12 GHz) for each receiver in each sideband, for a total of 32 GHz bandwidth, at a uniform 140 kHz resolution. We are currently expanding the correlator coverage by 50%, to 12 GHz bandwidth (IF coverage from 4 to 16 GHz) for each receiver in each sideband, for 48 GHz total bandwidth, while maintaining the fine 140 kHz uniform resolution. While not yet fully commissioned, we are working toward offering this new capability in 2020A as a shared-risk opportunity.

The SMA can tune the orthogonal receiver combinations independently, resulting in a very flexible frequency coverage capability. For example, observations can be made at 1.3 mm and 870 micron simultaneously (with many other configurations possible). One popular configuration allows the current 8 GHz/sideband/receiver frequency coverage to cover up to 32 GHz contiguously, where the tuning ranges overlap for the two orthogonally polarized receivers. Alternatively, the two receivers can be set with the same LO to cover the same 16 GHz (8 GHz in each sideband) of frequency space in the two orthogonally polarizations, allowing improved spectral line sensitivity. In such a case, full Stokes polarization measurements are also possible at 1.3 mm and 870 microns. When our upgrade is completed to 12 GHz/sideband/receiver, the frequency coverage will be configurable to cover 44 GHz contiguously (with 4 GHz of overlap), or can be configured to cover the same 24 GHz (12 GHz in each sideband) with the same LO.

The SMA provides flexible, wide band frequency coverage that delivers high continuum sensitivity and excellent spectral line capabilities. A full transit observation with the current 8 GHz/sideband/receiver correlator coverage will offer continuum sensitivity of 250 or 600 micro-Jy (1 sigma) at 230 or 345 GHz in good weather conditions (precipitable water vapor 2.5 mm and 1.0 mm, respectively). When the correlator upgrade is fully commissioned this will improve the continuum sensitivities by 22% per unit time. The corresponding line sensitivities at 1 km/s resolution are 35 and 80 mJy.

For more information about SMA capabilities, visit the **SMA Observer Center website (http://sma1.sma.hawaii.edu/status.html)** and explore the set of **SMA proposing tools (http://sma1.sma.hawaii.edu/tools.html).** Current and archived **SMA Newsletters (https://www.cfa.harvard.edu/sma/Newsletters/)** provide a sampling of the wide variety of science possible with the SMA.

For more details visit the SMA Observer Center Proposal Information Page at **http://sma1.sma.hawaii.edu/proposing.html**

IMPORTANT DATES FOR STANDARD OBSERVING PROPOSALS
Submissions open: **06 February 2020 (on or before)**
Submissions close: **05 Mar 2020 21:00 UTC / 05 Mar 2020 16:00 EST / 06 Mar 2020 05:00 Taiwan**

Due to current and expected investment in further upgrades to the SMA capabilities, as well as obligations to previous approved programs, the Large Scale Projects program (for projects requesting 100 to 1000 hours) will not be accepting proposals at this time.

Questions or comments regarding the Standard Observing Proposals can be addressed to **sma-propose@cfa.harvard.edu**.

Mark Gurwell
Chair, Submillimeter Array Time Allocation Committee

STAFF CHANGES IN HILO

Ryan Howie, Astrophysicist (Telescope Operator), left the SMA in September after twelve years of service. We thank Ryan for his efforts and wish him success in the future.

Johnathan Larson, Astrophysicist (Telescope Operator), left the SMA in September to take a position in the Department of the Army. We thank Johnathan for his efforts and wish him success in the future.

Clint Monceaux, Safety Specialist, joined SAO in August, reporting to Simon Radford. Previously Clint worked for the Department of the Navy at Pearl Harbor.

Fiona Smith, Astrophysicist (Telescope Operator), joined SAO in October. She recently earned her bachelor's degree in physics at the Renssellaer Polytechnic Institute.

PROPOSAL STATISTICS 2019B (16 NOV 2019 – 15 MAY 2020)

The SMA received a total of 59 proposals (SAO 42) requesting observing time in the 2019B semester. The proposals received by the joint SAO and ASIAA Time Allocation Committee are divided among science categories as follows:

CATEGORY	PROPOSALS
low/intermediate mass star formation, cores	13
high mass (OB) star formation, cores	11
local galaxies, starbursts, AGN	8
submm/hi-z galaxies	8
protoplanetary, transition, debris disks	7
GRB, SN, high energy	5
UH	3
Galactic center	2
other	2

TRACK ALLOCATIONS BY WEATHER REQUIREMENT (ALL PARTNERS):

PWV[1]	SAO	ASIAA	UH[2]
< 4.0mm	33A + 42B	4A + 5B	4
< 2.5mm	21A + 15B	6A + 5B	11
< 1.0mm	0A + 0B	0A + 2B	0
Total	**54A + 57B**	**10A + 12B**	**15**

(1) Precipitable water vapor required for the observations.

(2) UH does not list As and Bs.

TOP-RANKED 2019B SEMESTER PROPOSALS

The following is the listing of all SAO and ASIAA proposals with at least a partial A ranking with the names and affiliations of the principal investigators.

GALACTIC CENTER

Michael Johnson, SAO
Polarimetric VLBI with the Event Horizon Telescope

GRB, SN, HIGH ENERGY

Alexandra Tetarenko, East Asian Observatory
Constraining Jet Formation and Evolution with Transient X-ray Binaries

Anna Ho, Caltech
The death throes of massive stars, revealed through early millimeter observations

Kuiyun Huang, CYCU
New Insights in Short GRBs

HIGH MASS (OB) STAR FORMATION, CORES

Giuliana Cosentino, European Southern Observatory (ESO), University College of London (UCL)
G034.77-00.55 and the first fully resolved CJ-type interstellar shock.

Junhao Liu, Center for Astrophysics | Harvard & Smithsonian
A pilot dust polarization survey of massive dense cores in Cygnus-X

LOCAL GALAXIES, STARBURSTS, AGN

Gianluca Castignani, Ecole polytechnique fédérale de Lausanne
Environment effect in cosmic filaments: mapping CO in HI-deficient galaxies

Keiichi Asada, ASIAA
Origin of the accretion flow of M87

LOW/INTERMEDIATE MASS STAR FORMATION, CORES

Giulia Perotti, University of Copenhagen
Mind the gap: linking ice and gas around R CrA

Jia-Wei Wang, Academia Sinica Institute of Astronomy and Astrophysics
Probe the multi-scale magnetic fields within the intermdiate mass hub-filament system OMC2-FIR4

Manar el Akel, Observatory of Paris, LERMA
The Rosetta stone to sulfur: H2S from laboratory to observations

Naomi Hirano, ASIAA
Magnetic fields in the central regions of prestellar cores

PROTOPLANETARY, TRANSITION, DEBRIS DISKS

Dana Anderson, Caltech
An Exploration of Nitrogen Gas Content in Protoplanetary Disks (2018B-S046 Continuation)

Evan Rich, University of Michigan
Gmeini-LIGHTS Survey: Flux and Gas Dynamics of Never Before Observed Protoplanetary Disks

Feng Long, Smithsonian Astrophysical Observatory
The Synergy between SMA and ALMA: test disk formation and evolution models

Hau-Yu Baobab Liu, ASIAA
Millimeter Flux Variability/Stability of FU Orionis Objects and EXors

SUBMM/HI-Z GALAXIES

Attila Kovacs, SAO
Active Sunyaev-Zel'dovich clusters: sub-structure and starburst galaxies within

Garrett "Karto" Keating, SMA/SAO
Untangling the Molecular Mystery of An Unusual High-Redshift Galaxy

Joseph Cairns, Imperial College London
Cluster Cores at z > 4

Matthew Ashby, Harvard-Smithsonian Center for Astrophysics
The Impact of Radio Jets on Star Formation in AGN Host Galaxies, Part II

OTHER

Romane Le Gal, Harvard-Smithsonian Center for Astrophysics
First unbiased interferometric molecular survey of PDRs: NGC 7023 NW and 2023 S

SAO PROPOSALS 2019A SEMESTER

The following is the listing of all SAO proposals observed in the 2019A semester (16 May 2019 – 15 Nov 2019).

Nacho Añez, Institut de Ciències de l'Espai
What is controlling the fragmentation process?

Matthew Ashby, CfA
The Impact of Radio Jets on Star Formation in AGN Host Galaxies

Yusuke Aso, ASIAA
Pilot Survey of Deuterated Molecules in Class 0 Protostars (resubmission)

Henrik Beuther, Max-Planck-Institute for Astronomy
The importance of magnetic fields for the fragmentation of high-mass star-forming regions (the summer targets)

Andrew Burkhardt, CfA
A Deep, Broadband Interferometric Chemical Survey of L1157

David Clements, Imperial College London
A Rosetta Stone for Distant Dusty Star-Forming Galaxies: SERVS, Herschel and the SMA

Mark Gurwell, CfA
Full Polarization Thermal Mapping of Ganymede and Callisto

Mark Gurwell, CfA
Titan 1.1mm Band Spectral Line Imaging Survey

Anna Ho, Caltech
The death throes of massive stars, revealed through early millimeter observations

Jane Huang, CfA
A pilot wideband chemical survey of Class I protostellar disks (resubmission)

Todd Hunter, NRAO
Accretion outbursts in massive protostars: Monitoring of dust continuum and excited methanol masers in the third known source - G358.931-0.030

David Jewitt, UCLA
Extraordinary Distant Comet C/2017 K2

Tomasz Kaminski, CfA
The aftermath of a stellar collision in the Galactic Bulge

Tomasz Kaminski, CfA
What is K4-47? Investigating the Most Molecularly Complex Planetary Nebula to Date

Chia-Lin Ko, National Tsing Hua University
Abundance ratios of S-bearing molecules as an alternative probe of grain growth

Charles Law, CfA
Searching for Ionized Accretion Flows around 0.1 pc Scale Clusters with O-Type Stars

Hau-Yu Baobab Liu, ASIAA
Millimeter Flux Variability/Stability of FU Orionis Objects and EXors

Meredith MacGregor, Carnegie DTM
The Origin and Impact of Flares in M Dwarf Systems

Michael McCollough, CfA
Using SMA to probe the jet emission in microquasar Cyg X-3 during radio outburst

Keping Qiu, Nanjing University
Continuum emission from massive starless cores

Goran Sandell, University of Hawaii
The R Mon / NGC 2261 (Hubble's variable nebula) molecular outflow

Justin Spilker, University of Texas at Austin
A Complete Inventory of the Molecular ISM in a Starburst Galaxy at the Peak Epoch of Cosmic Star Formation

Yuji Urata, NCU
Search for Bright submm GRB afterglows Toward Radio Polarimetry

Laura D. Vega, Vanderbilt University
Hunting for Disks Around Pulsating RV Tau Stars

Jia-Wei Wang, ASIAA
Resolve the polarization morphology from the envelope to the Keplerian disk at 200 AU scale in the massive protostar Cepheus A HW2

Jonathan Williams, University of Hawaii
A Search for Water and Complex Organics around an Outbursting Star

Tomohiro Yoshida, ASIAA
ASIAA summer student program 2019A

RECENT PUBLICATIONS

TITLE: Formation of Massive Protostellar Clusters- Observations of Massive 70 μm Dark Molecular Clouds
AUTHOR: Li, Shanghuo; Zhang, Qizhou; Pillai, Thushara; Stephens, Ian W.; Wang, Junzhi; Li, Fei
PUBLICATION: *The Astrophysical Journal, Volume 886, Issue 2, article id. 130, 16 pp. (2019).*
PUBLICATION DATE: December 2019
ABSTRACT: https://ui.adsabs.harvard.edu/abs/2019ApJ...886..130L/abstract

---

TITLE: SMA Observations of Haro 2: Molecular Gas around a Hot Superbubble
AUTHOR: Beck, Sara C.; Hsieh, Pei-Ying; Turner, Jean
PUBLICATION: *eprint arXiv:1909.04971*
PUBLICATION DATE: September 2019
ABSTRACT: https://ui.adsabs.harvard.edu/abs/2019arXiv190904971B/abstract

---

TITLE: Sub-arcsecond (Sub)millimeter Imaging of the Massive Protocluster G358.93-0.03: Discovery of 14 New Methanol Maser Lines Associated with a Hot Core
AUTHOR: Brogan, C. L.; Hunter, T. R.; Towner, A. P. M.; McGuire, B. A.; MacLeod, G. C.; Gurwell, M. A.; Cyganowski, C. J.; Brand, J.; Burns, R. A.; Caratti o Garatti, A.; Chen, X.; Chibueze, J. O.; Hirano, N.; Hirota, T.; Kim, K. -T.; Kramer, B. H.; Linz, H.; Menten, K. M.; Remijan, A.; Sanna, A. Sobolev, A. M.; Sridharan, T. K.; Stecklum, B.; Sugiyama, K.; Surcis, G.; Van der Walt, J.; Volvach, A. E.; Volvach, L. N.
PUBLICATION: *The Astrophysical Journal Letters, Volume 881, Issue 2, article id. L39, 9 pp. (2019).*
PUBLICATION DATE: August 2019
ABSTRACT: https://ui.adsabs.harvard.edu/abs/2019ApJ...881L..39B/abstract

---

TITLE: Massive dust clumps in the envelope of the red supergiant VY Canis Majoris
AUTHOR: Kamiński, T.
PUBLICATION: *Astronomy & Astrophysics, Volume 627, id.A114, 12 pp.*
PUBLICATION DATE: July 2019
ABSTRACT: https://ui.adsabs.harvard.edu/abs/2019A%26A...627A.114K/abstract

---

TITLE: Ejection History of the IRAS 04166+2706 Molecular Jet
AUTHOR: Wang, Liang-Yao; Shang, Hsien; Chiang, Tzu-Yang
PUBLICATION: *The Astrophysical Journal, Volume 874, Issue 1, article id. 31, 12 pp. (2019).*
PUBLICATION DATE: March 2019
ABSTRACT: https://ui.adsabs.harvard.edu/abs/2019ApJ...874...31W/abstract

---

TITLE: Characterizing the Gamma-Ray Variability of the Brightest Flat Spectrum Radio Quasars Observed with the Fermi LAT
AUTHOR: Meyer, Manuel; Scargle, Jeffrey D.; Blandford, Roger D.
PUBLICATION: *The Astrophysical Journal, Volume 877, Issue 1, article id. 39, 30 pp. (2019).*
PUBLICATION DATE: May 2019
ABSTRACT: https://ui.adsabs.harvard.edu/abs/2019ApJ...877...39M/abstract

TITLE: Mass Assembly of Stellar Systems and their Evolution with the SMA (MASSES) -- Full Data Release
AUTHOR: Stephens, Ian W.; Bourke, Tyler L.; Dunham, Michael M.; Myers, Philip C.; Pokhrel, Riwaj; Tobin, John J.; Arce, Héctor G.; Sadavoy, Sarah I.; Vorobyov, Eduard I.; Pineda, Jaime E.; Offner, Stella S. R.; Lee, Katherine I.; Kristensen, Lars E.; Jørgensen, Jes K.; Gurwell, Mark A.; Goodman, Alyssa A.
PUBLICATION: *eprint arXiv:1911.08496*
PUBLICATION DATE: November 2019
ABSTRACT: https://ui.adsabs.harvard.edu/abs/2019arXiv191108496S/abstract

---

TITLE: Discovery of a New Class I Methanol Maser Transition at 266.8 GHz
AUTHOR: Chen, Xi; Ellingsen, Simon P.; Ren, Zhi-Yuan; Sobolev, Andrej M.; Parfenov, Sergey; Shen, Zhi-Qiang
PUBLICATION: *The Astrophysical Journal, Volume 877, Issue 2, article id. 90, 8 pp. (2019).*
PUBLICATION DATE: June 2019
ABSTRACT: https://ui.adsabs.harvard.edu/abs/2019ApJ...877...90C/abstract

---

TITLE: Ejection of Double Knots from the Radio Core of PKS 1510-089 during the Strong Gamma-Ray Flares in 2015
AUTHOR: Park, Jongho; Lee, Sang-Sung; Kim, Jae-Young; Hodgson, Jeffrey A.; Trippe, Sascha; Kim, Dae-Won; Algaba, Juan-Carlos; Kino, Motoki; Zhao, Guang-Yao; Lee, Jee Won; Gurwell, Mark A.
PUBLICATION: *The Astrophysical Journal, Volume 877, Issue 2, article id. 106, 10 pp. (2019).*
PUBLICATION DATE: June 2019
ABSTRACT: https://ui.adsabs.harvard.edu/abs/2019ApJ...877..106P/abstract

---

TITLE: The ISM Properties and Gas Kinematics of a Redshift 3 Massive Dusty Star-forming Galaxy
AUTHOR: Leung, T. K. Daisy; Riechers, Dominik A.; Baker, Andrew J.; Clements, Dave L.; Cooray, Asantha; Hayward, Christopher C.; Ivison, R. J.; Neri, Roberto; Omont, Alain; Pérez-Fournon, Ismael; Scott, Douglas; Wardlow, Julie L.
PUBLICATION: *The Astrophysical Journal, Volume 871, Issue 1, article id. 85, 29 pp. (2019).*
PUBLICATION DATE: January 2019
ABSTRACT: https://ui.adsabs.harvard.edu/abs/2019ApJ...871...85L/abstract

---

The Submillimeter Array (SMA) is a pioneering radio-interferometer dedicated to a broad range of astronomical studies including finding protostellar disks and outflows; evolved stars; the Galactic Center and AGN; normal and luminous galaxies; and the solar system. Located on Maunakea, Hawaii, the SMA is a collaboration between the Smithsonian Astrophysical Observatory and the Academia Sinica Institute of Astronomy and Astrophysics.

SUBMILLIMETER ARRAY
Center for Astrophysics | Harvard & Smithsonian
60 Garden Street, MS 78
Cambridge, MA 02138 USA
www.cfa.harvard.edu/sma/

SMA HILO OFFICE
645 North A'ohoku Place
Hilo, Hawaii 96720
Ph. 808.961.2920
Fx. 808.961.2921
sma1.sma.hawaii.edu

ACADEMIA SINICA INSTITUTE
OF ASTRONOMY & ASTROPHYSICS
11F of Astronomy-Mathematics Building,
AS/NTU, No. 1, Sec. 4, Roosevelt Road
Taipei 10617
Taiwan R.O.C.
www.asiaa.sinica.edu.tw/